Dynamical Structure, Bonding, and Thermodynamics of the Superionic Sublattice in α-AgI

Brandon C. Wood and Nicola Marzari
Department of Materials Science and Engineering, Massachusetts Institute of Technology, Cambridge, MA 02139

Using extensive first-principles molecular dynamics calculations, we characterize the superionic phase transition and the lattice and electronic structures of the archetypal Type-I superionic conductor α-AgI. We find that superionicity is signalled by a phase transition of the silver ions alone. In the superionic phase, the first silver shell surrounding an iodine displays a distinct dynamical structure that would escape a time-averaged characterization, and we capture this structure in a set of ordering rules. The electronic structure of the system demonstrates a unique chemical signature of the weakest-bound silver in the first shell, which in turn is most likely to diffuse. Upon melting, the silver diffusion decreases, pointing to an unusual entropic contribution to the stability of the superionic phase.

PACS numbers: 71.15.Pd,66.30.-h,66.30.Dn

Key advances in energy research have prompted a surge of interest in superionic materials, as a crucial enabling technology for a variety of nanotechnological devices, including sensors, switches, batteries, and fuel cells. Of the superionics, AgI and related silver halides and sulfides have attracted particular attention because of the unusually high levels of ionic conductivity they exhibit, and as such are finding increased and varied technological implementation [1, 2, 3]. At normal pressure, AgI enters its superionic α phase above $T_c = 420$ K, at which temperature a phase transition to a body-centered cubic structure is accompanied by an increase in the silver conductivity of nearly three orders of magnitude, to a value of 1.31 $\Omega^{-1}\,\mathrm{cm}^{-1}$ [4]. Previous molecular dynamics studies using classical pair potentials have successfully reproduced experimental characteristics of the α and β phases, as well as the $\alpha \rightarrow \beta$ transition [5, 6, 7, 8, 9, 10], but these are unable to describe the electronic structure in a dynamic environment, or to capture the phenomenology of the melting transition. In this regard, first-principles simulations provide unique and unbiased predictive power.

We perform Car-Parrinello molecular dynamics simulations in the canonical NVT ensemble at temperatures ranging from 200 K to 1250 K for a total of 800 ps. All simulations were performed with a 54-atom unit cell and $a_0 = 5.174$ Å, except the Wannier function calculations, which were performed in a 32-atom unit cell [21].

First, we find evidence of a phase transition of the silver ions near the experimental T_c that is independent of the conformation and dynamics of the iodine sublattice and signals the transition into the superionic α phase. The silvers exhibit a sharp decrease in their diffusion behavior upon cooling below T_c, although cubic boundary conditions forbid the iodine structural transition to the hexagonal wurtzite β phase. Results from a series of simulations in which we immobilized the iodines in a fixed bcc configuration provide a secondary, stronger indicator of the independence of the silver transition from any iodine dynamics. Fig. 1 displays the associated silver ion diffusion coefficients D_{Ag} for the fixed-iodine case and for a fully mobile lattice. Diffusion coefficients are derived from the mean-square displacement (MSD) via the Einstein relation, $D = \lim_{t\rightarrow\infty} \frac{1}{6t} \langle MSD(t) \rangle$. In both cases, the slope of an Arrhenius plot of D_{Ag} shows a characteristic discontinuity near the experimental transition temperature. Unexpectedly, this discontinuity is even more pronounced for the fixed-iodine case. Immobilizing the iodine sublattice does lead to an overall decrease in D_{Ag}, suggesting local lattice fluctuations beneficial for silver mobility are frozen out, but the system retains its superionic behavior.

Also of note in Fig. 1 is the unusual decrease of the silver ion diffusion coefficient upon melting at about 850 K, a tendency that has also been observed experimentally [4, 11] but is not captured by classical potentials. The thermodynamic implication gives valuable insight into the stability of the superionic phase. The decreased mobility of the silver ions upon melting signals a decrease in the silver entropic contribution, meaning the iodines crystallize into the superionic state below T_m to increase the entropy of the silvers and make them more "liquid". Accordingly, the superionic phase acts as an intermediate between a pure solid and a pure liquid, with a high-entropy liquid sublattice flowing through a low-energy solid matrix. An entropically driven stabilization of the α phase is also consistent with experimental results [12], which determine the entropy difference between superionic and liquid phases to be relatively tiny.

Although it is not possible to separate the total energy of the system into respective sublattice contributions, we can get a quantitative picture of the energetic fluctuations associated with each sublattice by instead integrating the forces on the ions, which are already decoupled. Since in the canonical ensemble, fluctuations σ in the total energy are related to the specific heat capacity C_V

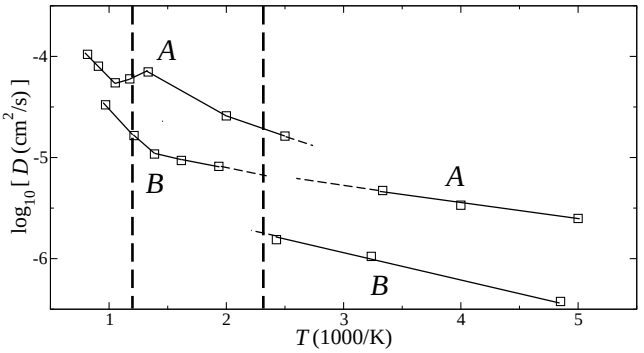

FIG. 1: Arrhenius plot of the diffusion coefficient for the fully mobile system (A) and with the iodine sublattice fixed (B). The dashed vertical lines indicate the experimental T_c (420 K) and T_m (830 K) at standard pressure.

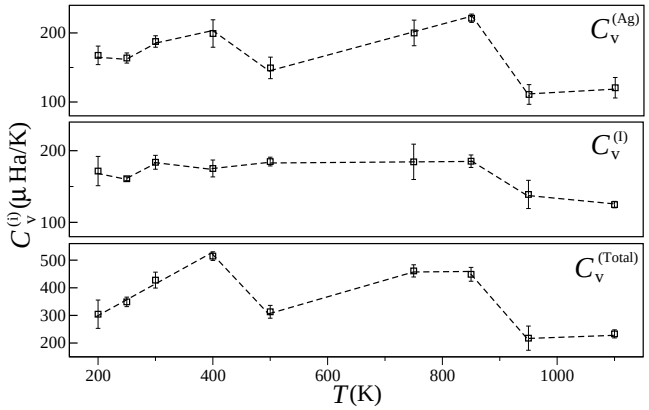

FIG. 2: Specific heat capacities for the silver sublattice, the iodine sublattice, and the total system.

as $\sigma^2 = \mathrm{k}_B T^2 C_V$, we can derive a heat capacity-like quantity $C_V^{(i)}$ that is sublattice resolved using the energetic fluctuations derived from the ionic forces. A plot of this quantity for the two sublattices, along with the total specific heat capacity for the entire system, is shown in Fig. 2. Over the full temperature range of the simulations, we observe the tail end of a divergence in the total heat capacity at 400 K and 850 K. These temperatures correspond closely to the superionic transition temperature T_c and the melting temperature T_m, respectively. Examination of the associated ion-resolved $C_V^{(i)}$ curves reveals a similar divergence for the silvers at T_c but no detectable trend for the iodines. As in Fig. 1, we can thus link the superionic transition to the silver sublattice only.

We note that an order-disorder transition of the silver ions at T_c has been reported previously [13, 14]. Our results confirm separation of the occupied tetrahedral sites into the six inequivalent sublattices of Ref. [15], the occupancies of which are plotted as a function of temperature in Fig. 3. The simulations reveal an ordering tendency for the silvers below T_c, characterized by a splitting into

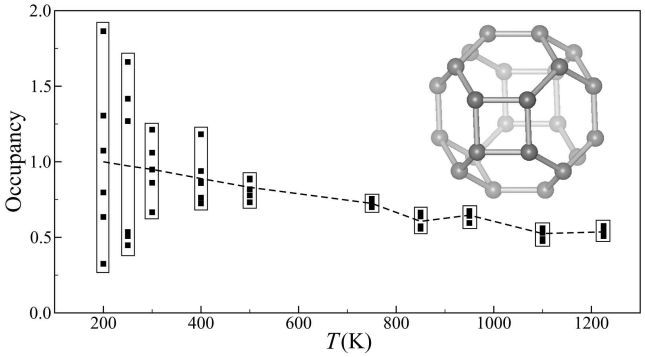

FIG. 3: Average silver occupancies of the six inequivalent tetrahedral bcc interstitial sublattices of Ref. [15], normalized against the case for which all ions occupy random tetrahedral sites. The inset shows the network of tetrahedral sites surrounding a single iodine, and the dashed line indicates the overall fraction of silvers in tetrahedral sites.

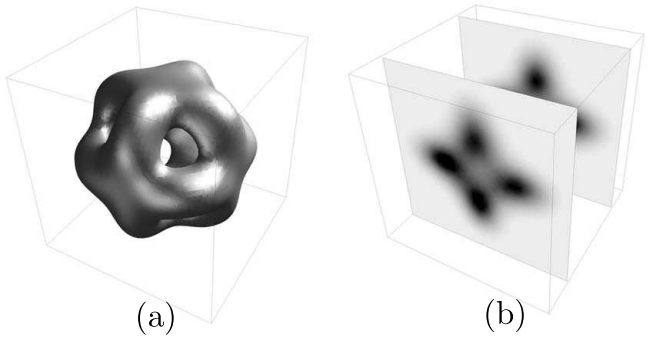

FIG. 4: (a) The isosurface of silver trajectories at 750 K, enclosing a volume associated with the first silver shell surrounding an iodine. (b) A slice plot of (a), revealing higher density (darker) silver occupancy regions.

higher- and lower-occupancy sublattices. The independent ordering tendency of the silver sublattice upon cooling is observable despite the inhibition of the $\alpha \rightarrow \beta$ transition, in agreement with Ref. [13]. However, at these low temperatures, even more extensive statistical sampling is necessary to allow for comparison of the ordered phase with those proposed in the cited studies.

We have also investigated the most frequented pathways for the silver ions by tracking their positions with respect to the iodines and averaging the resulting trajectories over the course of the simulations. Fig. 4 shows isosurface and slice plots for the silver ion density in the first shell surrounding an iodine. Our results confirm that the highest-density regions lie near the tetrahedral sites, with silver ion density smeared toward the octahedral sites. This agrees well with the experimental results of Ref. [16].

From the ionic trajectories, we can identify a set of rules governing the instantaneous distribution of silvers. The silver-silver pair distribution function $g_{Ag-Ag}(r)$

(Fig. 5) illustrates a zero probability of finding silver ions closer together than $R_{Ag-Ag} = 2.4$ Å, which precludes simultaneous occupation of nearest-neighbor tetrahedral interstitial sites. Integration of $g_{Ag-I}(r)$ over the first peak reveals that on average, each iodine has four nearest neighbors in the first shell, consistent with geometric expectations for tetrahedral interstitial site occupancy. In addition, $g_{Ag-I}(r)$ indicates the highest probability distance for silvers surrounding an iodine is at $R_{Ag-I} = 2.6$ Å, which corresponds to the radial distance to a tetrahedral interstitial site. However, a time-resolved analysis suggests a more detailed decomposition of the first peak of $g_{Ag-I}(r)$. We find that most commonly, three of the four nearest-neighbor silver ions simultaneously occupy a shell that corresponds to the tetrahedral site distance (the average value varies from 2.7 to 3.0 depending on temperature, with lower temperatures favoring higher values). The fourth silver is seen to transition regularly between this shell and an equivalent shell for a neighboring iodine such that on average, it fills the transition zone between the two, as defined by $2.8 \leq R_{Ag-I} \lesssim 4.2$ Å. The transitioning rate is temperature dependent and disappears rapidly for $T < T_c$. The fourth silver also possesses an angular distribution distinct from its three inner counterparts, as indicated in the inset of Fig. 5. The Ag–I–Ag angles for any of the closest three silvers reveal preferences at 65° and 105°, and higher angles are surprisingly uncommon. However, the angles introduced by the inclusion of the fourth nearest-neighbor shell are comparatively diffuse and have significant probabilities towards larger values. This suggests that whereas the closest three silvers are clustered and correlated in their positions, the fourth silver is relatively unconstrained in its angular configuration and is affected only marginally by the orientations of the remaining three. The rare permanent transitions of this unconstrained fourth silver between shells represent the driving factor for mass diffusion, an observation that would escape experimental investigations.

The above analysis allows for the definition of a set of ordering rules that govern the instantaneous distribution of silver ions in the first shell surrounding an iodine: (1) four silver ions populate the first shell; (2) no two silver ions occupy neighboring tetrahedral interstitial sites; (3) on average, three silver ions surround an iodine at a radius of $R_{Ag-I} = 2.6$ Å, the tetrahedral interstitial distance; (4) a fourth silver transitions between that shell and a second shell at $R_{Ag-I} \gtrsim 4.2$ Å, associated with a neighboring iodine, and the transition rate between the two is temperature dependent and disappears below T_c; (5) the angular positions of the three inner silvers are correlated, with preferred Ag–I–Ag angles of 65° and 105°, whereas the fourth (outer) silver is relatively unconstrained; and (6) silver ions tend to organize into high- and low-occupancy sublattices at temperatures below T_c.

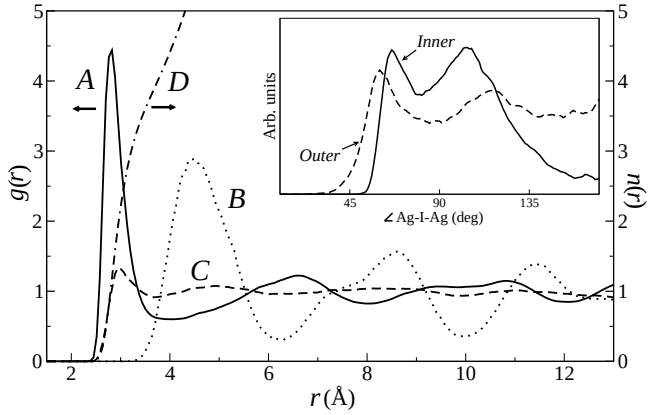

FIG. 5: Radial pair distribution functions for (A) Ag–I, (B) I–I, and (C) Ag–Ag, along with the integrated Ag–I $n(r)$ curve (D), at 750 K. Inset shows the angular distributions of the four silver ions in the first shell surrounding an iodine, measured with respect to the remaining silvers in the shell and resolved according to the three innermost silvers and the fourth outer silver.

We examined the maximally localized Wannier functions (MLWFs) to obtain a local picture of bonding in a dynamic environment [17]. Plotting the time-averaged radial distribution of the four iodine Wannier function centers (WFCs) about their parent ion reveals an unexpected bimodal separation into short-distance, highly localized WFCs and longer-distance, partially delocalized WFCs (Fig. 6). Further isolating Wannier functions associated with each of the two peaks and plotting the time- and statistical-averaged contours for the WFCs around the iodines yields the isosurfaces shown in the insets of Fig. 6. The long-distance Wannier function centers (LWFCs) tend to align along the cubic axes toward the octahedral interstitial sites. Their orientations relate to the observed smearing of the silver occupancy from the electrostatically preferred tetrahedral sites towards the octahedral face centers and suggest that these orbitals correspond to directional interactions between silvers and iodines. On the other hand, the short-distance iodine Wannier function centers (SWFCs) exhibit a random angular distribution, as would be expected in a strictly Coulombic picture. Comparing the areas of the two peaks in Fig. 6 reveals that of the four WFCs surrounding an iodine, 30% on average can be classified as SWFCs, a figure which agrees with the likelihood for a first-shell silver to be found in the mobile transition zone. This value also correlates well with the the experimentally determined likelihood of a silver to be located outside the tetrahedral interstitial site [16, 18], a quantity confirmed by our findings.

A more detailed picture of the correlation between delocalization extent of the iodine MLWFs and the positions of nearby silver atoms is offered in Fig. 7. There is clear evidence of a chemical interaction between LWFCs

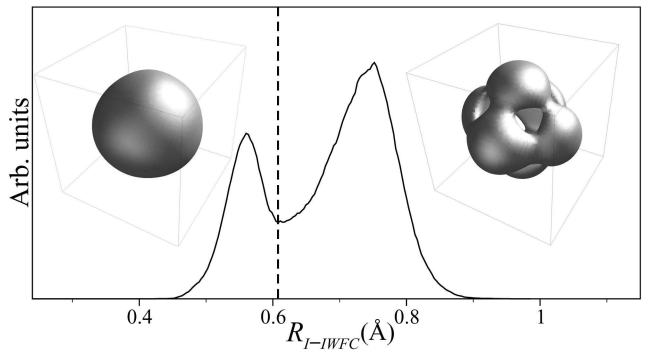

FIG. 6: Histogram of distances between iodine WFCs and iodine nuclei. The insets are contours of the iodine WFC distribution about their nuclei for WFCs on either side of the broken line.

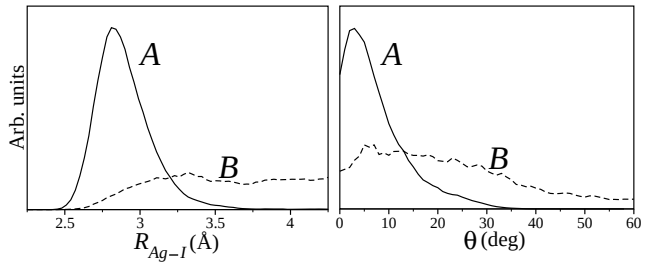

FIG. 7: Histograms of interionic bond distance and bond angle for the silvers closest to iodine WFCs, resolved into (A) long-distance and (B) short-distance Wannier functions. The bond angle θ is defined as the angle between $\boldsymbol{R}_{Ag-I}$ and $\boldsymbol{R}_{IWFC-I}$.

and silver atoms within a threshold radius of $R_{Ag-I} \lesssim 3.25$ Å and a solid bond angle of $|\theta| \lesssim 20°$. This positional constraint on the silvers indicates the bonding with LWFCs is directional and not merely Coulombic. As a quantitative measure of these more complex chemical interactions, we have also calculated the Born effective charges for the ionic sublattices, using the electric-enthalpy method of Refs. [19]. We obtain values of $Z^* = \pm 1.22$, larger than the integral values expected for a purely ionic crystal, further supporting the conclusions of our Wannier function analysis. Fig. 7 shows no such directional interaction for SWFCs, indicating that corresponding interactions with silvers can be attributed to weaker electrostatics. Moreover, examination of the radial distribution for first-shell silvers closest to SWFCs places them within the transition zone.

We conclude that silvers contributing to D_{Ag} are those which are not bound to LWFCs, meaning they are minimally constrained both radially and angularly. Most commonly, the outermost of the four first-shell silvers fills these criteria, as a lack of stronger directional interactions with LWFCs increases the average Ag–I bond distance. This comparatively unconstrained, mobile fourth silver fleetingly occupies the transition zone defined by $2.8 \leq R_{Ag-I} \lesssim 4.2$ Å until it is captured by a neighboring iodine, leading to mass diffusion. At higher temperatures, thermal disordering breaks a greater number of bonds between silvers and LWFCs, promoting more nearby silvers into the transition zone. As such, the overall fraction of occupied tetrahedral sites decreases (Fig. 3) and diffusion is enhanced.

In conclusion, we have shown that the transition to the superionic α phase of AgI is signalled by an independent phase transition of the silver sublattice alone, characterized by a disordering of the silvers and a sharp increase in their diffusivity. Upon melting, the silver diffusion coefficient decreases, pointing to an unusual entropic contribution to the stabilization of the superionic phase. We have also identified diffusion pathways for superionic silver ions above T_c, and a time-resolved analysis of ion trajectories has allowed us to define a set of ordering rules that govern the instantaneous distribution of silvers in the first shell surrounding an iodine. Finally, we have found that of the four first-shell silvers, the closest three are strongly correlated and restricted in their angular distribution, and that they are involved in anisotropic, directional bonding to an iodine. The fourth silver is bound only weakly and is relatively unconstrained, and we have isolated it as the dominant contributor to mass diffusion.

Funding for this work has been provided by the DOE CSGF fellowship and MURI Grant DAAD 19-03-1-0169. Calculations have been done with the Quantum-ESPRESSO package [20] using computational facilities provided through NSF grant DMR-0414849. The authors also wish to thank Prof. Bernhard Wuensch for helpful discussions.

[1] K. Terabe et al., Nature **433**, 47 (2005).
[2] M. Lee et al., Appl. Phys. Lett. **85**, 3552 (2004).
[3] T. Minami et al., Solid State Ion. **86-8**, 415 (1996).
[4] A. Kvist and A. M. Josefson, Z. Naturforsch. **23a**, 625 (1968).
[5] P. Vashishta and A. Rahman, Phys. Rev. Lett. **40**, 1337 (1978); M. Parrinello et al., Phys. Rev. Lett. **50**, 1073 (1983).
[6] F. Shimojo and M. Kobayashi, J. Phys. Soc. Jpn. **60**, 3725 (1991).
[7] K. O'Sullivan et al., Phys. Rev. B **43**, 13536 (1991).
[8] F. Zimmer et al., J. Chem. Phys. **112**, 6416 (2000).
[9] J. L. Tallon, Phys. Rev. B **38**, 9069 (1988).
[10] For reviews on the subject, see S. Hull, Rep. Prog. Phys. **67**, 1233 (2004); D. A. Keen, J. Phys. Cond. Matt. **14**, R819 (2002).
[11] H. Araki et al., J. Phys. Soc. Jpn. **68**, 134 (1999).
[12] W. Biermann and W. Jost, Z. Phys. Chem. (Frankfurt am Main) **17**, 139 (1960).
[13] P. A. Madden et al., Phys. Rev. B **45**, 10206 (1992).
[14] C. Seok and D. W. Oxtoby, Phys. Rev. B **56**, 11485 (1997); Phys. Rev. B **58**, 5146 (1998).

[15] G. Szabó, J. Phys. C **19**, 3775 (1986).
[16] R. J. Cava et al., Solid State Commun. **24**, 411 (1977).
[17] N. Marzari and D. Vanderbilt, Phys. Rev. B **56**, 12847 (1997).
[18] V. M. Nield et al., Solid State Ion. **66**, 247 (1993).
[19] P. Umari and A. Pasquarello, Phys. Rev. Lett. **89**, 157602 (2002); I. Souza et al., Ibid., 117602.
[20] S. Baroni et al., URL `http://www.quantum-espresso.org/`.
[21] Simulations were performed in a plane-wave basis set using the PBE-GGA XC functional, a $4d^{10}5s^1$ ultrasoft silver and $5s^25p^5$ norm-conserving iodine pseudopotential, cutoffs of 22 Ry and 176 Ry for the wavefunctions and charge density, and a timestep of 20 au.